

## Friction of water slipping in carbon nanotubes

Ming D. Ma,<sup>1</sup> Luming Shen,<sup>2,\*</sup> John Sheridan,<sup>3</sup> Jefferson Zhe Liu,<sup>3</sup> Chao Chen,<sup>1</sup> and Quanshui Zheng<sup>1,\*</sup>

<sup>1</sup>Department of Engineering Mechanics and Center for Nano and Micro Mechanics, Tsinghua University, Beijing 100084, China

<sup>2</sup>School of Civil Engineering, University of Sydney, NSW 2006, Australia

<sup>3</sup>Department of Mechanical and Aerospace Engineering, Monash University, Clayton, VIC 3800, Australia

(Received 10 August 2010; revised manuscript received 31 January 2011; published 31 March 2011)

Liquid slip is essential in nanofluidic systems, as shrinking channel size leads to a dramatic increase in flow resistance and thus high-energy consumption for driving nonslip flow. Using large-scale nonequilibrium molecular dynamics simulation of water flowing in carbon nanotubes (CNT's), we show that the relationship between the CNT wall-water interfacial friction stress and slip velocity follows a transition-state-theory-based inverse hyperbolic sine function, which remains universally valid regardless of wetting properties, CNT chiralities, and CNT sizes, and holds for all slip velocities from 0 to 1400 m/s. The finding could benefit the research in desalination and other chemical purification techniques.

DOI: 10.1103/PhysRevE.83.036316

PACS number(s): 47.61.-k, 47.63.mh, 66.20.-d

### I. INTRODUCTION

In nanofluidic systems, the interactions between the fluid molecules and the solid walls dominate the hydrodynamic behavior of the fluid [1–3]. The relation between the water-wall shear stress  $\tau$  and water slip velocity  $v_s$  is the key for characterizing the slip flow and implementing it into applications [3]. An alternative concept is the “slip length,”  $l_s$ , which is defined as the distance between the wall and an imaginary nonslip boundary, and can be correlated to  $\tau$  and  $v_s$  in the form of  $\tau = \mu v_s / l_s$ , where  $\mu$  is the water viscosity coefficient [3]. If  $l_s$  is constant, then  $\tau$  depends linearly upon  $v_s$  assuming that  $\mu$  is independent on flow velocity. This linear relationship was first proposed by Navier [4] a long time ago but has never been truly proved. In contrast, nonconstant slip lengths have been reported for many kinds of liquids, including water, using molecular dynamics (MD) simulations [5–7], indicating nonlinear  $\tau - v_s$  relations.

Recently, it has been reported that the flow rates in a bundle of carbon nanotubes or nanopipes are several orders of magnitude higher than those predicted by using conventional nonslip flow theory through pores that are nanometers in diameter [8–10]. It was suggested that these high fluid velocities become possible because of a frictionless surface at the carbon-nanotube wall [11]. The observations have provided an experimental basis for studying the boundary condition of possible water slipping at atomically smooth surfaces and for understanding the slip mechanisms of water, which remains a challenging task due to its unique polar molecule structure. A thorough understanding of the mechanism of water slip at the CNT wall is of great importance to nanofluidic research [2] because of its potential applications in desalination and other chemical purification devices [12].

Based on their nonequilibrium MD simulations for water flowing in CNT's, a parabolic relation  $\tau \propto v_s^{0.5}$  was recently proposed by Chen *et al.* [6]. Under the same pressure drops as those used in experiments, however, this parabolic relationship [6] leads to the predictions of  $\tau$  several orders of magnitude

higher than those measured in experiments [9,10]. We note that the simulation data points used may be insufficient to establish a reliable  $\tau - v_s$  relationship due to the low signal-to-noise ratios in the MD simulations of water flow at room temperature. Moreover, the simulated flow rate range (on the order of 5 ~ 300 m/s) [6] was much higher than those measured in experiments (0.01 ~ 0.05 m/s) [9]. Large extrapolations are thus required in order to compare the predicted and experimentally measured flow rates, which could result in large discrepancies.

Here we carry out comprehensive nonequilibrium MD simulations on slip flow of water inside CNT's, where a large amount of data are collected to generate statistically converged results. Our MD simulation results and the detailed investigation on the trajectories of the water molecules in the first layer within the CNT reveal an inverse hyperbolic sine (IHS) relationship between the CNT wall-water interfacial friction stress  $\tau$  and slip velocity  $v_s$ . This relation appears to be universally valid regardless of wetting properties, CNT chiralities, and CNT sizes, and holds for all slip velocities from 0 to 1400 m/s. Subjected to the pressure drop in experiments, the flow rate predicted from the proposed IHS relation agrees with the value measured experimentally very well. As the IHS relation is based on the transition state theory [13], the good agreement of such an IHS relation with our MD simulations results suggests that the thermal activation process dominates the flow behavior of water flowing in CNT's. Detailed analysis of the trajectories of the water molecules in the first liquid layer in our MD simulations also supports this mechanism.

### II. ATOMIC SIMULATIONS

To get a reliable  $\tau - v_s$  relation, we carry out large-scale nonequilibrium MD simulations for water transporting in double-walled CNT's at a flow rate ranging from 0.8 to 1400 m/s. In the simulations, double-walled CNT's are employed, with flexible innertubes and rigid outertubes. The carbon atoms in innertubes are modeled by the reaction bond order potential [14] and subject to van der Waals interactions with the atoms in outertubes. Since the moduli of the membrane matrix materials silicon nitride [9] and anodic

\*Corresponding authors: Luming.Shen@sydney.edu.au; zhengqs@tsinghua.edu.cn

aluminum oxide [8] (i.e., 255 GPa [15] and 141 GPa [16], respectively) are much higher than the effective modulus between the inner and outer tubes, i.e.,  $\sim 36.5$  GPa [17], it is reasonable to assume the outertubes to be rigid. The TIP3P model [18] is adopted for the water. We characterize the interaction between water and carbon atoms by a standard 6-12 Lennard-Jones (LJ) potential  $V(r) = 4\epsilon[(\sigma/r)^{12} - (\sigma/r)^6]$ , where  $r$  is the distance between the carbon and oxygen atoms,  $\epsilon$  is the well depth of the potential, and  $2^{1/6}\sigma$  is the equilibrium carbon-oxygen distance. By measuring the density profile of a water droplet on a graphene layer as used in Werder *et al.* [19], we estimate the contact angle of water on graphene for a given LJ potential model for the oxygen-carbon interaction. For contact angles of  $45^\circ/91^\circ/135^\circ$ , with  $\sigma$  fixed at 0.319 nm, the  $\epsilon$  is estimated to be  $5.849/4.063/1.95$  meV, respectively. A 30-nm-long CNT is modeled and periodic boundary conditions are applied along the CNT axial direction.

Using  $\pi(R-d)^2L$ , where  $R$  and  $L$  are the inner radius and length of the CNT's, respectively, and  $d = 0.31$  nm is the average distance between the first layer of water molecules and the innertube as the occupied volume [20], the number of water molecules inside the nanotube is chosen to maintain the initial water density of  $998 \text{ kg/m}^3$ , resulting in a total of  $\sim 3400$  water molecules in a double-walled carbon nanotube system, (20,20)@(25,25). The cutoff distances for the van der Waals interactions and the real-space part of the Coulomb interactions are set to be 1 nm. The long-range Coulomb interactions are described by using the particle-particle particle-mesh technique with a root-mean-square accuracy of  $10^{-4}$ . All the MD simulations are carried out using the code LAMMPS [21]. The simulations are in time steps of 1 fs. The initial structures are obtained after 100-ps equilibration under a constant temperature of 298 K for both water and the innertube to reach the thermoequilibrium state under an NVT ensemble. After the initial equilibration, a constant force of 0.12 pN is applied to each water molecule to accelerate the flow inside the tube, as shown in Fig. 1(a). During this process, the temperature of the innertube is maintained at 298 K, while the temperature of the flowing water is not controlled.

The flow rate,  $v(t)$ , at time  $t$  is defined as the mean value of the axial velocities of all water molecules over a properly chosen time interval,  $\Delta t$ , ended at  $t$ . In other words,  $v(t)$  is the velocity of the center of mass of the water group concerned. The acceleration,  $a(t)$ , is obtained using  $[v(t + \Delta t) - v(t - \Delta t)]/(2\Delta t)$ . According to Newton's second law, the instantaneous interfacial frictional stress  $\tau(t)$  is thus equal to  $[F - Ma(t)]/(\pi DL)$ , where  $F$  is the total force applied onto all the water molecules,  $M$  is the total mass of the water, and  $D$  ( $= 2.7$  nm) and  $L$  ( $= 30$  nm) are the innertube diameter and cell length, respectively. In this paper, we refer to the above-mentioned relation between  $\tau$  and  $v$  as the  $\Delta t$ -averaged  $\tau - v$  relation.

### III. RESULTS AND DISCUSSION

#### A. Data processing

The density profile reported in Fig. 1(b) indicates that water molecules form layered structures within the CNT. Figure 1(c) shows the typical profiles (dots) of the axial

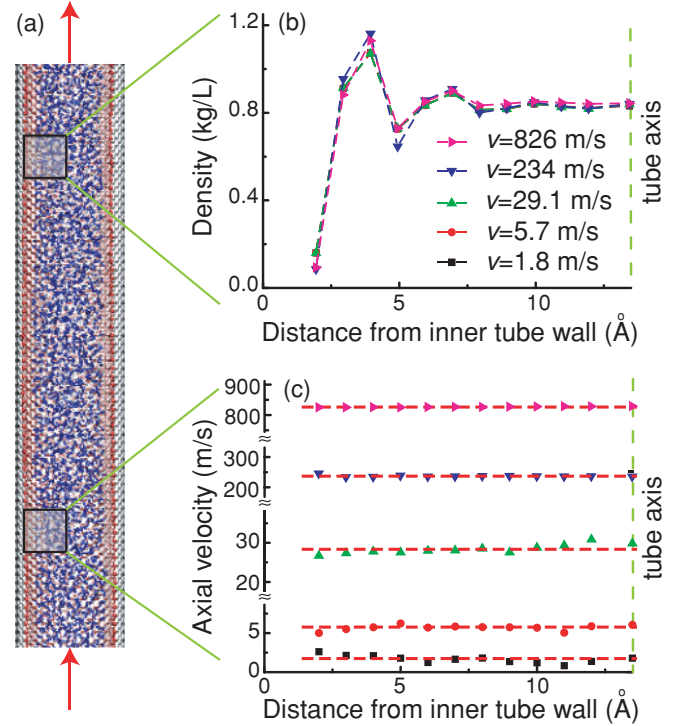


FIG. 1. (Color online) (a) Schematic illustration of water transporting in a double-walled carbon nanotube (DWCNT). The outer tube (black) is fixed, and the inner tube (red) is flexible and its temperature is maintained at 298 K. (b) Radial density profile of water inside DWCNT's at various flow rates. (c) Radial velocity profiles (dots) at various flow rates, the dashed lines are the corresponding mean velocities.

velocity components of water molecules at various flow rates along the radial direction in the (20,20)@(25,25) tube with the CNT-water model corresponding to a  $91^\circ$  contact angle. The dashed lines are the corresponding mean velocities  $v$ . These pluglike flow velocity profiles suggest the average flow speed in the CNT and the slip velocity at the CNT wall to be almost the same, which is consistent with observations in the works of Chen *et al.* [6] and Joseph *et al.* [22], and the conclusions drawn by Hanasaki *et al.* [23]. It is therefore reasonable to claim that the  $\tau - v$  and  $\tau - v_s$  relations are exchangeable in this study.

At room temperature, it is estimated that the average speed of water molecules driven by thermofluctuations is  $\sim 340$  m/s, which results in a very low signal-to-noise ratio (SNR) at low flow speeds. According to the central limit theorem [24], the deviation of  $\tau - v_s$  curves is proportional to  $(\Delta t)^{-1/2}$  and  $(N)^{-1/2}$ , where  $N$  is the mean sample number. Two techniques are thus adopted to obtain high signal-to-noise ratio data, particularly at low flow speeds.

The first method is to do the time average. The black solid line and blue triangles in Fig. 2(a) are the typical plots of 1- and 10-ps-averaged  $\tau - v$  relations, respectively. It is evident that a longer time average leads to a smaller fluctuation or less "noise." This observation agrees with the central limit theorem [24], which states that the deviation is proportional to  $(\Delta t)^{-1/2}$ . Although a longer time average is more effective in filtering out the noise, it will also reduce the number of

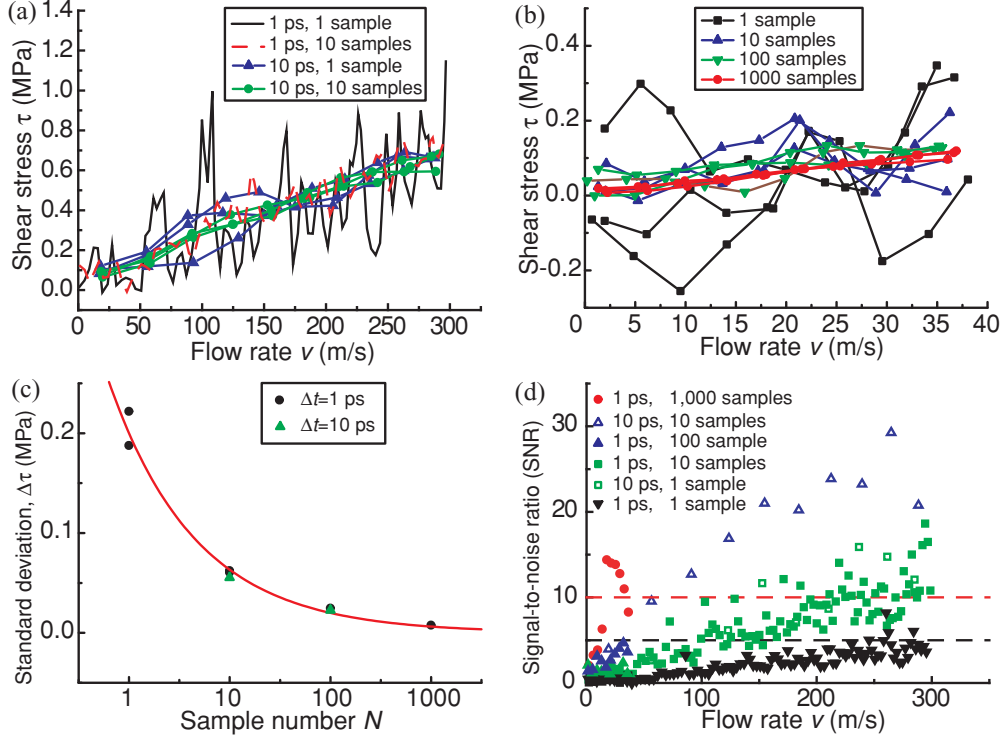


FIG. 2. (Color online) Sample-mean method for getting reliable data from MD simulations for the  $\tau - v$  relation. (a) The decrease of deviation with the increase of sample time or sample number. (b) The dependence of deviation on the number of sample used. (c) The flow-rate independent theoretical (solid line, predicted using central limit theorem [23]) and calculated standard deviations of  $\tau$  at temperature 298 K. (d) The corresponding signal-to-noise ratio (SNR) for averages based on different time intervals and sample numbers (symbols), compared with two expected levels, 5 and 10 (dashed lines).

data points and thus lead to a loss of resolution. In this case, we need the second method, which employs a large number of independent simulations. Mean values of average speed  $v$  and shear stress  $\tau$  are then calculated over these independent samples. The curves in Fig. 2(b) show the very large deviation of 1-ps-averaged  $\tau$  at low flow rates, and the rapid reduction of the deviation with the increasing independent sample number. Figure 2(c) shows that the deviation of  $\tau - v$  curves is proportional to  $N^{-1/2}$ , which is consistent with the central limit theorem [24]. The solid line in Fig. 2(c) shows the relation predicted by the central limit theorem between the deviations, defined by  $\Delta\tau = \sqrt{[\sum_{i=1}^N \tau_i^2 - (\sum_{i=1}^N \tau_i)^2/N]/(N-1)}$ , and the mean sample number  $N$ , where the data points are the calculated ones corresponding to the plots in Figs. 2(a) and 2(b). The obvious drawback of the second method is the heavy computational effort. In this study a combination of these two techniques was used.

To get a reliable relation between  $\tau$  and  $v$ , a sufficiently high signal-to-noise ratio (say,  $>5$ ) is required, particularly in the very low flow speed range. A systematic study of the effects of the two averaging techniques mentioned in the preceding paragraph was performed. The results are summarized in Fig. 2(d). The symbols in Fig. 2(d) show the calculated SNR vs the flow rate, as compared with two expected levels (5 and 10) represented by two dashed lines. From Fig. 2(d), we find that in the low flow rate range of 0–40 m/s, more than 1000 independent simulations are required for  $\text{SNR} > 5$ . For larger

flow rates, the 10-ps time-averaged approach is able to increase the SNR ratio above the expected value (say, 10) using a limited number of independent computational samples. Hence, we average 100 independent simulations at the moderate flow rates of 50–250 m/s, and use one sample at the high flow rates of 300–1400 m/s.

### B. Inverse hyperbolic sine function

Over 10,000 independent MD simulations of water flowing through an armchair double-walled CNT (20,20)@(25,25) are performed with the water-CNT interaction model corresponding to one of the three different contact angles of 45°, 91°, and 135°, which cover the range of contact angles investigated by many researchers except for 0° [19]. The obtained  $\tau - v_s$  data points (dots) are plotted in Fig. 3(a) for flow rates ranging from 0.8 to 1400 m/s. After careful examination, we find that the obtained results [data points in Fig. 3(a)] are not linear and deviate from the analytical expression  $\tau \sim v^{0.5}$  proposed by Chen *et al.* [6]. Instead, all of these results can be fitted very well using a general inverse hyperbolic sine relation  $(\tau - \tau_c)/\tau_0 = \text{arcsinh}(v_s/v_s^0)$  with  $\tau_c$ ,  $\tau_0$ , and  $v_s^0$  being three fitting parameters, which has been proposed recently based on the transition state theory [13]. In this relation,  $\tau_c$  is the critical shear stress that liquid molecules must overcome in order to move from one stable state to another. Recent experimental observations [8] and theoretical analysis [25] suggest that the shear stress  $\tau$  goes to zero when  $v_s$  approaches zero for

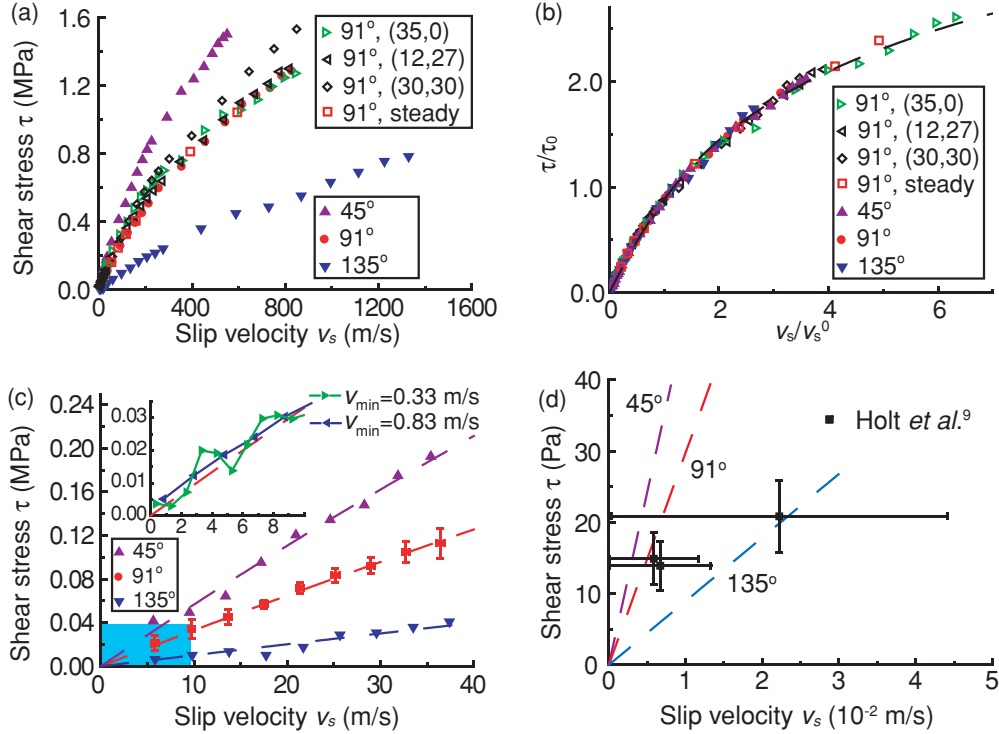


FIG. 3. (Color online) (a) Relationship between the interfacial frictional stresses  $\tau$  and slip velocity  $v_s$  with different water contact angles ( $91^\circ$ ,  $45^\circ$ ,  $135^\circ$ ), diameters, and loading manners. (b) The normalized simulation values of shear stress ( $\tau/\tau_0$ ) vs  $v_s/v_s^0$  with respect to carbon nanotubes. The corresponding least square fits in a unified IHS function form of  $\tau/\tau_0 = \text{arcsinh}(v_s/v_s^0)$ . (c) A closer look at the relations in the slip speed range of 0–40 m/s. The inset shows the convergence of 10,000-sample means with a contact angle of  $91^\circ$  based on 0.25- (rightward triangles), and 0.5- ps-averaged (leftward triangles)  $\tau$  for the first 2.5 ps, which correspond to the shaded area spanning from 0 to 10 m/s. (d) Comparison between the experimentally observed data (dots) [9] and the IHS relationship prediction (dashed lines). The chirality of the inner tube is (20,20) unless specified.

liquid flowing over atomic-scale smooth surfaces. Our MD simulation results confirm that the value of  $\tau_c$  is negligible, which suggests that the  $\tau - v_s$  curve passes through the (0, 0) point indeed. Further discussion on this issue will be presented later.

By applying the least-squares fitting technique to the simulated data points and the origin (0,0), we can then express the general inverse hyperbolic sine function in the form

$$\tau/\tau_0 = \text{arcsinh}(v_s/v_s^0), \quad (1)$$

which agrees very well with all of the simulation results in the entire flow rate range of 0.8–1400 m/s, as shown in Fig. 3(b). The corresponding values of  $\tau_0$  and  $v_s^0$  are listed in Table I. An enlarged picture for the low-slip speed range (<40 m/s) is shown in Fig. 3(c), which also shows a reasonable fitting. Furthermore, we examine the 10,000-sample means of 0.25- and 0.5-ps-averaged  $\tau$  over the first 2.5 ps of simulation time. The results (dots with solid lines) are shown in the inset of Fig. 3(c) where they are compared with the proposed IHS relation predication (dashed lines). It is clear that this proposed IHS relation still holds at average flow speeds down to 0.83 m/s. We also checked the effects of the water density [26]. The water density is chosen to vary from 945 to 1169 kg/m<sup>3</sup> with the occupied volume defined above. Under a given flow speed, less than 10% deviation is observed in the shear stress

as compared with the results obtained using water density of 998 kg/m<sup>3</sup>. This difference is comparatively small compared with the effect of the contact angle. Besides that, all of the results can be well described by the proposed arcsinh relation [Eq. (1)].

Due to the excessively long simulation time required in order to get large number of  $\tau - v_s$  data from steady state flows, our simulation data were obtained from unsteady state flows. To directly compare our simulations with experiments, we need to investigate whether the MD simulation results obtained under nonsteady state are still valid for steady state loading, under which the experimental results were measured under given pressure drops [8–10]. In our MD simulation, we thus carry out steady state simulation by applying forces with different magnitude to water molecules. The  $\tau - v_s$  relations are obtained after the flow has reached its steady state, i.e., the

TABLE I. Fitted parameters in the inverse hyperbolic sine relationship,  $\tau/\tau_0 = \text{arcsinh}(v_s/v_s^0)$

Inner tube	(20,20)			(12,27)		
	45°	91°	135°	(35,0)	91°	(30,30)
$\tau_0$ (MPa)	0.743	0.583	0.45	0.488	0.615	0.911
$v_0$ (m/s)	153	196	504	133	209	315
$l_s^0 = \mu v_0^0 / \tau_0$ (nm)	205	336	1120	272	339	345

flow rate no longer changes with respect to time. It is found that the  $\tau - v_s$  relation obtained from the steady state flow [open squares in Fig. 3(a)] coincides with that under nonsteady state [solid dots in Fig. 3(a)]. In other words, the simulation results are not sensitive to whether they are obtained from steady state flows or not. Thus, our calculated shear stress  $\tau$  at the CNT-water interface can be easily related to pressure drop  $P$  by using  $\tau = PR/(2L)$  in the steady state flow, where  $R$  is the radius of the CNT tunnel and  $L$  is the membrane thickness.

To check the validity of the proposed IHS relationship for different kinds of CNT's, double-walled CNT's with similar inner diameters but different chiralities [e.g., (35,0)@(25,25) and (12,27)@(25,25)] and CNT's with larger inner diameters [e.g., (30,30)@(35,35)] are also investigated using MD simulations. The results are shown in Fig. 3(a). It is found that the proposed IHS relation still holds for the flows in these CNT's [Fig. 3(b)], and the corresponding values of  $\tau_0$  and  $v_s^0$  are reported in Table I.

The solid squares in Fig. 3(d) are the data points reproduced from the experiments of Holt *et al.* [9]. The comparison with the prediction (the dashed line) based on the proposed IHS relation [Eq. (1)] shows a reasonable agreement between the prediction and experimental data even at the very low flow rate range of  $0.5 - 5.0 \times 10^{-2}$  m/s.

A qualitative explanation on the obtained relation [Eq. (1)] could shed light on understanding the underlying physical mechanisms. It is well established that the size confinement in the nanochannel leads to the ordering tendency of liquid molecules next to the solid wall. It is thus proposed that the slip flow at the interface is mediated by the diffusion of atomic vacancies in the first liquid layer [25]. The pluglike speed profile also suggests that the flow of water molecules inside CNT's be a collective diffusion instead of the viscous flow. The proposed IHS  $\tau - v_s$  function, which is derived based on the transition state theory [13], is consistent with such molecular mechanism. It is worth noting that this relation holds for flow speed up to several hundred meters per second.

### C. Negligible critical shear stress

One question remains: Is the critical stress  $\tau_c$  in the original IHS negligible? Although Navier's prediction [4] as well as the recent experimental observations [8] and theoretical

analysis [25] suggest that the shear stress  $\tau$  goes to zero when  $v_s$  approaches zero for liquid flowing over atomic-scale smooth surfaces, to the best of our knowledge, there has been no directly experimental, theoretical, or numerical proof of it up until now. Due to the thermal noise in the fluid flow, it is not feasible to directly address this question by progressively reducing the slip velocity down to zero in our MD simulation (say, about  $10^{-2}$  m/s as the one measured in the experiment of Holt *et al.* [9]). Here we will only provide a qualitative understanding.

In order to find out whether  $\tau_c$  could be neglected, we traced the trajectory of each water molecule near the CNT wall. The contact angle of the water on the CNT wall is chosen as  $91^\circ$  unless otherwise indicated. Figure 4(a) demonstrates the residual probabilities of the first layer of water molecules. The residual probability is defined as the percentage of the water molecules present at the first layer at time  $t = 0$  and remaining until time  $t$ . As a function of time, it is clear from the figure that all the water molecules in the first layer will leave the first layer after about 70 ps at temperatures above 298 K, regardless of flow velocity and contact angle. We find that with a larger contact angle, the water molecules are more likely to leave that layer, which is consistent with our intuition. Figure 4(b) reports that the potential distance of each water molecule within the first layer can travel during a time period of 20 ps under zero flow rate and  $T = 298$  K. It appears that due to the thermal activation, almost all water molecules in the first layer can move out of the potential energy well formed by the CNT-water interaction at room temperature, which suggests that the critical shear stress  $\tau_c$  would be very small in our simulation. This phenomenon can also be understood in terms of the Maxwell model for viscoelasticity [27]. It is well accepted that the relaxation time, the mean lifetime of a liquid molecule in its equilibrium position, determines the observed viscous or viscoelastic fluid behavior. It is believed that the fluid with short relaxation time on the order of picoseconds cannot stand any static shear strain or exhibit any viscous behavior, i.e., following the traditional Newton's constitutive relation [27]. From Fig. 4(a), it can be estimated that the Maxwell relaxation time of the first layer of water is on the order of 5–10 ps, which implies a negligible  $\tau_c$ .

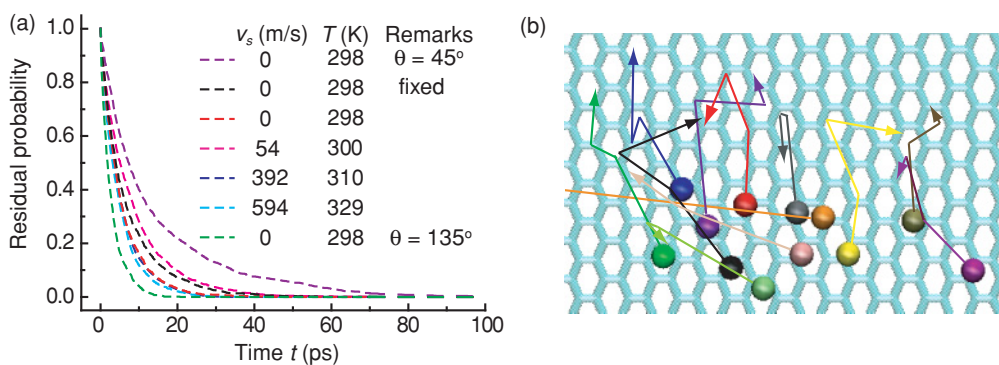


FIG. 4. (Color online) (a) Residual probabilities of water molecules in the first layers (contact angle =  $91^\circ$ ). The dashed lines mean the water molecules that are present in the first layer at time  $t = 0$  and never jump out of the first layer. The inner tube of (20,20)@(25,25) DWCNT is flexible and its temperature is maintained at 298 K unless specifically pointed out (i.e., fixed). (b) Possible distance each water molecule within the first layer can travel during a time period of 20 ps (time interval = 5 ps).

### D. Significance of the IHS relation

Next, we will relate the proposed IHS relation to some of the well-established quantities in the traditional hydrodynamic models and demonstrate that the new general relationship can not only serve as a good starting point to reveal the underlying physical mechanism in terms of the interfacial friction, but also be used as the “slip” boundary condition in hydrodynamic modeling of such nanofluidic systems. Since the values of  $v_s^0$  are hundreds of meters per second as shown in Table I, the linearization of Eq. (1),

$$\tau = kv_s, \quad (2)$$

is a good approximation at low flow rate range when  $v_s \ll v_s^0$ , where the dynamic friction coefficient  $k$  is associated with  $\tau_0$  and  $v_s^0$  as

$$k = \tau_0/v_s^0. \quad (3)$$

Slip length is another widely used quantity to describe the slip boundary condition. The slip length is defined as  $l_s = \mu v_s/\tau$  [3], where  $\mu$  is the viscosity coefficient of the bulk water. Together with Eq. (1), the slip length  $l_s$  can be determined by the IHS relationship in the form of

$$l_s/l_s^0 = \frac{v_s/v_s^0}{\operatorname{arcsinh}(v_s/v_s^0)}, \quad (4)$$

where

$$l_s^0 = \frac{\mu v_s^0}{\tau_0} = \frac{\mu}{k}. \quad (5)$$

According to Eq. (4), slip length  $l_s$  is a function of flow slip speed. At low flow slip speed, the values of  $l_s$  are almost constant ( $l_s^0$ ), which is simply the ratio of bulk viscosity  $\mu$  to the dynamic friction coefficient  $k$  [3]. The slip length of low rate flows derived from our MD simulations using Eq. (5) is also listed in Table I, which ranges from 200 nm to 1.1  $\mu\text{m}$  and shows a good agreement with the experimentally measured values ranging from 140 nm to 1.4  $\mu\text{m}$  [9]. Here we would like to stress that at nanoscale, when we consider the transport phenomenon, the slip length is not a well-defined concept. At nanoscale, it is well known that the interfacial properties dominate the transport behavior of water at solid surfaces, especially for friction. The slip length  $l_s$ , however, is not an interfacial property [3]. Despite its flow-rate-dependent properties as shown in Eq. (4), at low flow rate, it is actually the ratio of a bulk property—the viscosity of water  $\mu$ —to an interfacial property—the friction  $k$  as shown in Eq. (5). In contrast, the relationship between interface shear stress  $\tau$  and

slip velocity  $v_s$  as shown in Eq. (1) is intrinsically an interfacial property.

### IV. SUMMARY

In this paper, we performed MD simulations of water transporting through double-walled CNT's over a wide flow speed range (0.8–1400 m/s) with flexible innertubes. Through averaging large numbers of independent MD runs, e.g., 10,000, statistically converged data on the relationship between shear stress and flow slip speed were obtained at speeds as low as 0.8 m/s. Our simulation results reveal an inverse hyperbolic sine relationship between the CNT-water interfacial shear stress and slip velocity, which is universally valid regardless of wetting properties, tube chiralities, and diameters. The detailed investigation of the trajectories of the water molecules in the first layer within the CNT suggests that the proposed IHS relationship holds for the flow slip speed down to zero. The predictions based on this IHS relationship are also in good agreement with experimental observations [9].

By modeling the slip flow as a diffusion process, the IHS relationship is derived based on the transition state theory, in which several assumptions are adopted, such as low Knudsen number, two-dimensional model, nondeformable solid, and so on [13]. The good agreement between the fitted IHS analytical function and the experimental results indicate water slip at the interface as a thermal-activated diffusion process. The obtained pluglike speed profile and our detailed analysis on the water molecule trajectory in our MD also confirm this conclusion.

Furthermore, the proposed IHS relationship provides a quantitative slip boundary condition for investigating the hydrodynamic behavior of such nanofluidic systems, and could serve as a basis to study the underlying physical mechanisms of the experimental observations. The traditional concept of “slip length” can be derived from our IHS friction relationship as well.

### ACKNOWLEDGMENTS

This work is supported by the National Science Foundation of China (NSFC) through Grants No. 10672089, No. 10772100, No. 10832005, the 973 Program Grant No. 2007CB936803, and the IBM World Community Grid project “Computing for Clean Water.” Some of the MD simulations were carried out on the supercomputers in the Victorian Partnership for Advanced Computing (VPAC) and the NCI National Facilities in Australia.

- 
- [1] M. Robbins, *Nature* **389**, 331 (1997).
  - [2] L. Bocquet and E. Charlaix, *Chem. Soc. Rev.* **39**, 1073 (2010).
  - [3] L. Bocquet and J. L. Barrat, *Soft Matter* **3**, 685 (2007).
  - [4] C. L. M. H. Navier, *Mémoires de l'Académie Royale des Sciences de l'Institut de France* **6**, 389 (1823).
  - [5] A. Martini, H. Y. Hsu, N. A. Patankar, and S. Lichten, *Phys. Rev. Lett.* **100**, 4 (2008).
  - [6] X. Chen, G. X. Cao, A. J. Han, V. K. Punyamurtula, L. Liu, P. J. Culligan, T. Kim, and Y. Qiao, *Nano Lett.* **8**, 2988 (2008).
  - [7] P. A. Thompson and S. M. Troian, *Nature* **389**, 360 (1997).
  - [8] M. Whitby, L. Cagnon, M. Thanou, and N. Quirke, *Nano Lett.* **8**, 2632 (2008).
  - [9] J. K. Holt, H. G. Park, Y. M. Wang, M. Stadermann, A. B. Artyukhin, C. P. Grigoropoulos, A. Noy, and O. Bakajin, *Science* **312**, 1034 (2006).

- [10] M. Majumder, N. Chopra, R. Andrews, and B. J. Hinds, *Nature* **438**, 44 (2005).
- [11] J. A. Thomas and A. J. H. McGaughey, *Nano Lett.* **8**, 2788 (2008).
- [12] M. A. Shannon, P. W. Bohn, M. Elimelech, J. G. Georgiadis, B. J. Marinas, and A. M. Mayes, *Nature* **452**, 301 (2008).
- [13] F. Q. Yang, *Chemical Engineering Communications* **197**, 544 (2010).
- [14] D. W. Brenner, O. A. Shenderova, J. A. Harrison, S. J. Stuart, B. Ni, and S. B. Sinnott, *J. Phys. Condens. Matter* **14**, 783 (2002).
- [15] R. L. Edwards, G. Coles, and W. N. Sharpe, *Experimental Mechanics* **44**, 49 (2004).
- [16] S. Ko, D. Lee, S. Jee, H. Park, K. Lee, and W. Hwang, *Thin Solid Films* **515**, 1932 (2006).
- [17] B. T. Kelly, *Physics of Graphite* (Applied Science, London and New Jersey, 1981).
- [18] W. L. Jorgensen, J. Chandrasekhar, J. D. Madura, R. W. Impey, and M. L. Klein, *J. Chem. Phys.* **79**, 926 (1983).
- [19] T. Werder, J. H. Walther, R. L. Jaffe, T. Halicioglu, and P. Koumoutsakos, *J. Phys. Chem. B* **107**, 1345 (2003).
- [20] J. A. Thomas and A. J. H. McGaughey, *J. Chem. Phys.* **128**, 084715 (2008).
- [21] S. Plimpton, *J. Comput. Phys.* **117**, 1 (1995).
- [22] S. Joseph and N. R. Aluru, *Nano Lett.* **8**, 452 (2008).
- [23] I. Hanasaki and A. Nakatani, *J. Chem. Phys.* **124**, 144708 (2006).
- [24] W. Feller, *An Introduction to Probability Theory and Its Applications* (Wiley, New York, 1968).
- [25] A. Martini, A. Roxin, R. Q. Snurr, Q. Wang, and S. Lichter, *J. Fluid Mech.* **600**, 257 (2008).
- [26] See supplemental material at [<http://link.aps.org/supplemental/10.1103/PhysRevE.83.036316>] for the effects of the water density and variations of the pressure and density with respect to time. For more information on EPAPS, see [<http://www.aip.org/pubservs/epaps.html>].
- [27] D. J. Evans and G. Morriss, *Statistical Mechanics of Nonequilibrium Liquids* (Cambridge University Press, New York, 2008).